Lightweighting large optomechanical structures in astronomy instrumentation utilising generative design and additive manufacturing

James T. Wells, Marcell Westsik, Younes Chahid, Alastair Macleod, Lawrence Bissell, Richard Kotlewski, Scott McPhee, Jonathan Orr, Misael Pimentel Espirindio e Silva, Scott McKegney, William Cochrane, Ciar´an Breen, and Carolyn Atkins

Published version information:

Citation: James T. Wells, Marcell Westsik, Younes Chahid, Alastair Macleod, Lawrence Bissell, Richard Kotlewski, Scott McPhee, Jonathan Orr, Misael Pimentel Espirindio e Silva, Scott McKegney, William A. Cochrane, Ciarán Breen, Carolyn Atkins, "Lightweighting large optomechanical structures in astronomy instrumentation utilising generative design and additive manufacturing," Proc. SPIE 12669, Optomechanical Engineering 2023, 126690K (28 September 2023)

DOI: https://doi.org/10.1117/12.2676776

PROCEEDINGS OF SPIE

SPIEDigitalLibrary.org/conference-proceedings-of-spie

Lightweighting large optomechanical structures in astronomy instrumentation utilising generative design and additive manufacturing

James Wells, Marcell Westsik, Younes Chahid, Alastair Macleod, Lawrence Bissell, et al.

James T. Wells, Marcell Westsik, Younes Chahid, Alastair Macleod, Lawrence Bissell, Richard Kotlewski, Scott McPhee, Jonathan Orr, Misael Pimentel Espirindio e Silva, Scott McKegney, William A. Cochrane, Ciarán Breen, Carolyn Atkins, "Lightweighting large optomechanical structures in astronomy instrumentation utilising generative design and additive manufacturing," Proc. SPIE 12669, Optomechanical Engineering 2023, 126690K (28 September 2023); doi: 10.1117/12.2676776

SPIE.

Event: SPIE Optical Engineering + Applications, 2023, San Diego, California, United States

Lightweighting large optomechanical structures in astronomy instrumentation utilising generative design and additive manufacturing

James T. Wells[a,b], Marcell Westsik[a,c], Younes Chahid[a], Alastair Macleod[a], Lawrence Bissell[a], Richard Kotlewski[a], Scott McPhee[a], Jonathan Orr[d], Misael Pimentel Espirindio e Silva[d], Scott McKegney[d], William Cochrane[a], Ciarán Breen[a], and Carolyn Atkins[a]

[a]UK Astronomy Technology Centre, Royal Observatory, Edinburgh, EH9 3HJ, UK
[b]Dept of Mechanical Engineering, The University of Sheffield, Sheffield, S1 3JD, UK
[c]Dept of Mechanical, Aerospace, and Civil Engineering, The University of Manchester, Manchester, M13 9PL, UK
[d]Digital Factory, National Manufacturing Institute Scotland, University of Strathclyde, Glasgow, UK

ABSTRACT

Ground-based astronomical instruments have mass limits to ensure they can operate safely and accurately. Reducing the mass of optomechanical structures relieves mass budget for other components, improving the instrument's performance. Many industries have adopted generative design (GD) and additive manufacturing (AM; 3D printing) to produce lightweight components. This is yet to be implemented in ground-based astronomical instrumentation; this paper aims to provide insight into the advantages and limitations of this approach. The project studied the Extremely Large Telescope (ELT) Mid-infrared Imager and Spectrograph (METIS) three-mirror anastigmat (TMA); comparing the conventional, subtractive machined design with GD-AM designs. The TMA was selected due to its bespoke geometry constrained by an optical path, a conventional design which did not consider mass reduction, the size of the part (615 mm × 530 mm × 525 mm) that necessitated a study of different AM methods, and the operational environment (70 K & 10^{-6} Pa).

The study created mass-optimised designs of the TMA using topology optimisation and field-driven design. The performance of these designs was analysed using finite element analysis and optical ray tracing. It was found that GD-AM designs pass the required optical, structural and modal requirements, with a greater than 30% weight reduction when compared to the conventional design. The study investigated wire arc additive manufacturing (WAAM), a viable method of manufacturing components of the TMA's size. To commence the validation of WAAM for cryogenic environments, samples of WAAM aluminium 5356 were created and studied. The internal and external dimensions of two samples were investigated using X-ray computed tomography and the outgassing rate of two sets of three samples were evaluated to quantify the difference between machined and as-built samples.

Keywords: additive manufacturing, 3D printing, generative design, wire arc additive manufacturing, optomechanical structures

1. INTRODUCTION

Additive manufacturing (AM; 3D printing) is the process of manufacturing components by adding material, usually layer by layer, instead of the conventional subtractive manufacturing processes of milling and turning. Subtractive manufacturing methods require tool access to remove material and manufacture a component's

Further author information: (Send correspondence to C.A.)
C.A.: E-mail: carolyn.atkins@stfc.ac.uk
J.T.W.: E-mail: jtwells1@sheffield.ac.uk

Optomechanical Engineering 2023, edited by Keith B. Doyle, Brandon D. Chalifoux, Kenneth R. Castle, José M. Sasián, Proc. of SPIE Vol. 12669, 126690K
 · 0277-786X · doi: 10.1117/12.2676776

features. A key advantage of AM is removing the need for tool access, increasing design freedom, and allowing for the manufacturing of complex, freeform geometries.

The ASTM standard for AM terminology defines seven categories of AM.[1] One category is powder bed fusion (PBF), an AM method that uses focused thermal energy (from a laser or an electron beam) to selectively melt and fuse a powdered metal to form a part. Currently, PBF is the most readily available form of metal AM[2] and has been explored for use in ground-based astronomy instrumentation.[3] PBF is limited in build volume; a typical build bounding box is approximately 200 mm × 200 mm × 200 mm. Some machines now have build volumes reaching 1m in dimensions,[4] but these machines are very costly and not commercially available.

To manufacture large ($> 0.5\,\mathrm{m} \times > 0.5\,\mathrm{m} \times > 0.5\,\mathrm{m}$) metallic components with freeform geometries, a different category of AM is available, direct energy deposition (DED). DED uses focused thermal energy to melt a feed material onto a part. Unlike PBF, DED machines are not limited by the need to fill the build volume with powder. Large-scale parts are being made using DED at Relativity Space, MX3D, MER corporation, AML3D and AMFG.[5] Although DED has its disadvantages, namely that parts often contain material defects such as porosity, it can manufacture large freeform components on the metre and multi-meter scale.

In this paper, we investigated wire arc AM (WAAM), a form of DED. In WAAM, thermal energy from an arc, similar to that used in arc welding, is used to heat a metal wire and deposit it into a weld pool. The arc torch and wire feed are connected to a robotic arm, which moves to deposit material onto a build path, constructing a part. WAAM is a relatively inexpensive DED technology, with machine costs of £50,000 to £100,000 and wire feed material costs of £10 to £100/kg.[6] WAAM can produce large parts on the meter to multi-meter scale with fast build rates; Addilan, a manufacturer of DED machines, claims deposition rates of 6kg/hour.[7]

As ground-based astronomy instrumentation meets the demands of the next generation of 30 m class telescopes, there is increasing pressure on constraining the mass of instruments. It is challenging to keep instrumentation design under their mass limit while designing for multiple operational modes, each with tight performance requirements. This challenge has resulted in a desire for a method of designing and manufacturing lightweight, stiff structures. Using generative design (GD) tools to create mass-optimised designs and the increased design freedom of AM technologies, structural components can be lighter while maintaining performance, relieving the mass budget for other components.

In previous studies, Heidler et al.[8] demonstrated that topology optimisation and AM can be used to reduce the mass of an optical housing for a space application by 20% and Frasch et al.[3] used generative design tools to optimise the design of the structure for a three-mirror beam expander. In Frasch et al. the original component was $150\,\mathrm{mm} \times 90\,\mathrm{mm} \times 90\,\mathrm{mm}$ weighing 0.5 kg. They optimised the design with two different approaches; incorporating a stochastic lattice, reducing part mass by 30%; and implementing topology optimisation, reducing part mass by 23%. They went on to manufacture both designs using PBF.

Many structural components in modern ground-based astronomy instruments are larger than the examples discussed, for which the option of manufacturing the design using PBF is not feasible, hindering the exploration of AM in the ground-based astronomy instrumentation sector. Frank et al.[9] discussed the manufacturing of a supporting arm for an upgraded guiding probe for the Very Large Telescope. This component was manufactured using a non-metallic AM mold to cast the aluminium structure. This method would allow the manufacturing of complex large components; however, the increase in manufacturing steps would introduce more complexity and cost to the manufacturing process. It is possible to manufacture large components directly using AM. In March 2023, Relativity Space launched Terran 1, a rocket manufactured 85% by weight using AM. The 33 m fuselage of the Terran 1 was manufactured using AM with a custom WAAM machine capable of manufacturing components up to 9 m tall.[10]

This paper examines the use of WAAM to print large ($> 0.5\,\mathrm{m} \times > 0.5\,\mathrm{m} \times > 0.5\,\mathrm{m}$) optomechanical structures for ground-based astronomy instrumentation, investigating the feasibility of creating mass-optimised large components with WAAM technology. To investigate this, the paper will follow a case study for an optomechanical structure in ground-based astronomy instrumentation introducing the requirements of the case study in Section 2. Then, in Section 3, two design optimisation methods will be presented. Finally, in Section 4 will discuss the metrology and outgassing properties of samples manufactured from aluminium alloy 5356 using WAAM.

2. CASE STUDY BACKGROUND

The case study investigated a redesign of the structure of the three mirror anastigmat (TMA) in the extremely large telescope (ELT) mid-infrared ELT imager and spectrograph (METIS). The TMA structure supports three mirrors and a prism unit as shown in Figure 1. The structure is made from aluminium 6061 and consists of two machined parts and 28 fasteners with a combined mass of 27.6 kg. The TMA structure is 615 mm × 530 mm × 525 mm in size and operates at 70 K and 10^{-6} Pa. A conventional, subtractive machined design, shown in Figure 1, has been approved for manufacture and passes the design requirements defined by the European Southern Observatory (ESO). This design was created using conventional computer-aided design (CAD) software.

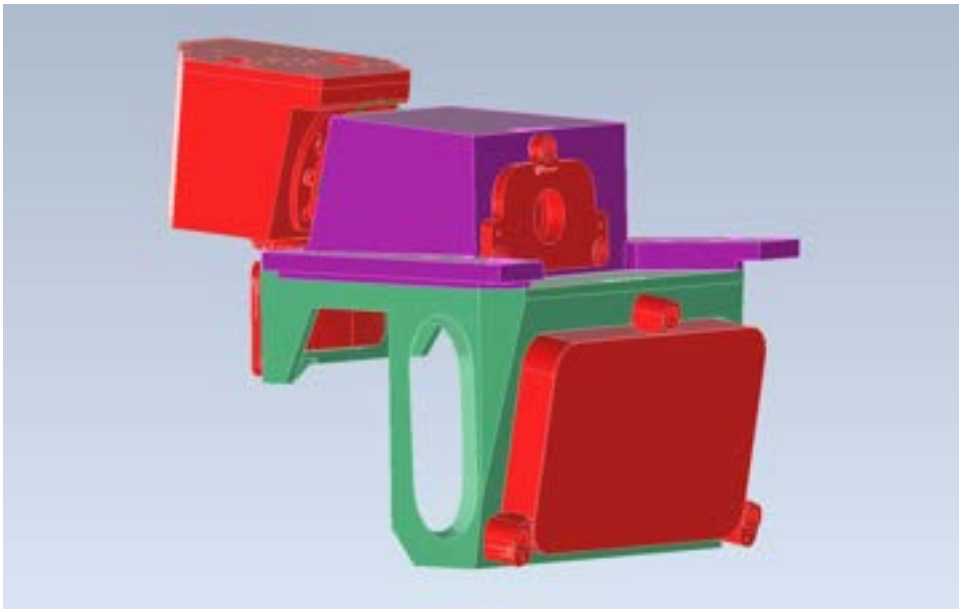

Figure 1. The three mirror anastigmat. Red bodies represent optical components; three mirrors and a prism unit. The green and purple bodies represent the TMA structure that supports the optical components, the part to be redesigned.

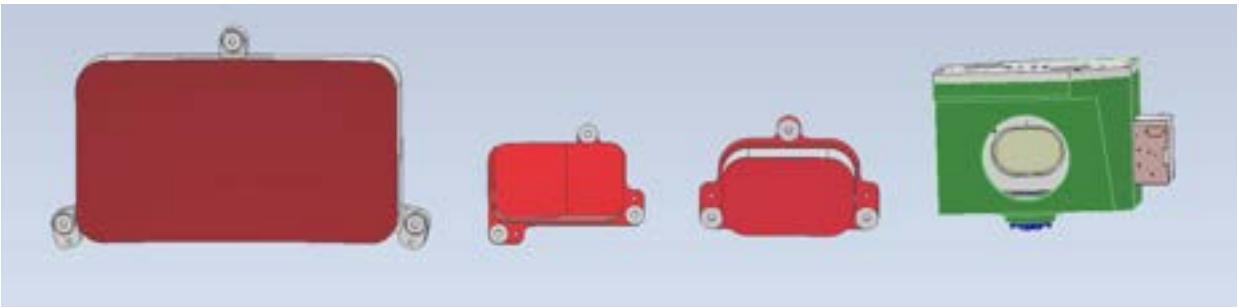

Figure 2. Optical components in the three-mirror anastigmat. From left to right; mirror one (M1), mirror two (M2), mirror three (M3) and the prism unit.

Designs presented in this paper will incorporate the same optical component design as the conventional TMA. Shown individually in Figure 2, these optical components are termed M1, M2, M3 and Prism in this paper. The optical components in this assembly must maintain a high level of alignment, so requirements were defined for the structure to ensure that; the structure does not plastically deform and; the optical components do not deform or move to the detriment of the optical performance. These requirements were defined at a variety of environments,

including operating (70 K & 10^{-6} Pa), storage (ambient temperature), and transport (ambient temperature and gravity acting in a different vector). Not all requirements for the component were considered in this case study. All design requirements for the TMA structure are shown in Table 1, which defines which requirements were tested for in this study and how they were tested.

Table 1. Requirements of the TMA[11]

Loading case	**Pass criteria**	**Evaluation within case study**
Shock loading during transport	Required $<$ 228 MPa Target $<$ 136 MPa	-
Quasi-static earthquake equivalency Storage environment (Equations 1 to 3)	Required $<$ 228 MPa Target $<$ 136 MPa	-
Quasi-static earthquake equivalency Operational environment (Equations 1 to 3)	Required $<$ 228 MPa Target $<$ 136 MPa	Finite element analysis
Standard gravity loading Operational environment	Required $<$ 228 MPa Target $<$ 136 MPa	-
Modal Eigenfrequency Operational environment	Required $>$ 28 Hz Targeted $>$ 70 Hz	Finite element analysis
Standard gravity loading Operational environment	Wavefront error $<$ 34 nm	Finite element analysis, Zernike fitting & ray tracing (Zemax)
Standard gravity loading Operational environment	Focal plane offset $<$ 100 µm Pupil plane offset $<$ 100 µm	-

$$A_{Ed1} = \pm E_{dx} \pm 0.3 \cdot E_{dy} \pm 0.3 \cdot E_{dz} \quad (1)$$

$$A_{Ed2} = \pm 0.3 \cdot E_{dx} \pm E_{dy} \pm 0.3 \cdot E_{dz} \quad (2)$$

$$A_{Ed3} = \pm 0.3 \cdot E_{dx} \pm 0.3 \cdot E_{dy} \pm E_{dz} \quad (3)$$

E_{dx} Quasi-static earthquake acceleration in x direction = 3.6g
E_{dy} Quasi-static earthquake acceleration in y direction = 3.6g
E_{dz} Quasi-static earthquake acceleration in z direction = 3.6g

3. DESIGN FOR ADDITIVE MANUFACTURE

The design of a component is often constrained by the manufacturing method it will use, for example, tool and jigging access; this restricts the geometry the component can take. AM methods often provide a reduction in these manufacturing constraints, enabling the creation of more complex, freeform components. When designing a component for AM, generative design tools are often used to optimise designs and explore the increased freedom AM offers. An example of a generative design tool is topology optimisation.

3.1 Topology optimised design

Topology optimisation is a group of generative design algorithms which iteratively optimise designs using simulation results, for example, results from finite element analysis. In the case of a structural component optimising for mass reduction, the topology optimisation simulates a structural loading scenario and then uses the results to statistically weight the importance of elements in the mesh. The higher the weighting of an element, the more structurally significant the mass of that element is. After performing this over many iterations, a body is

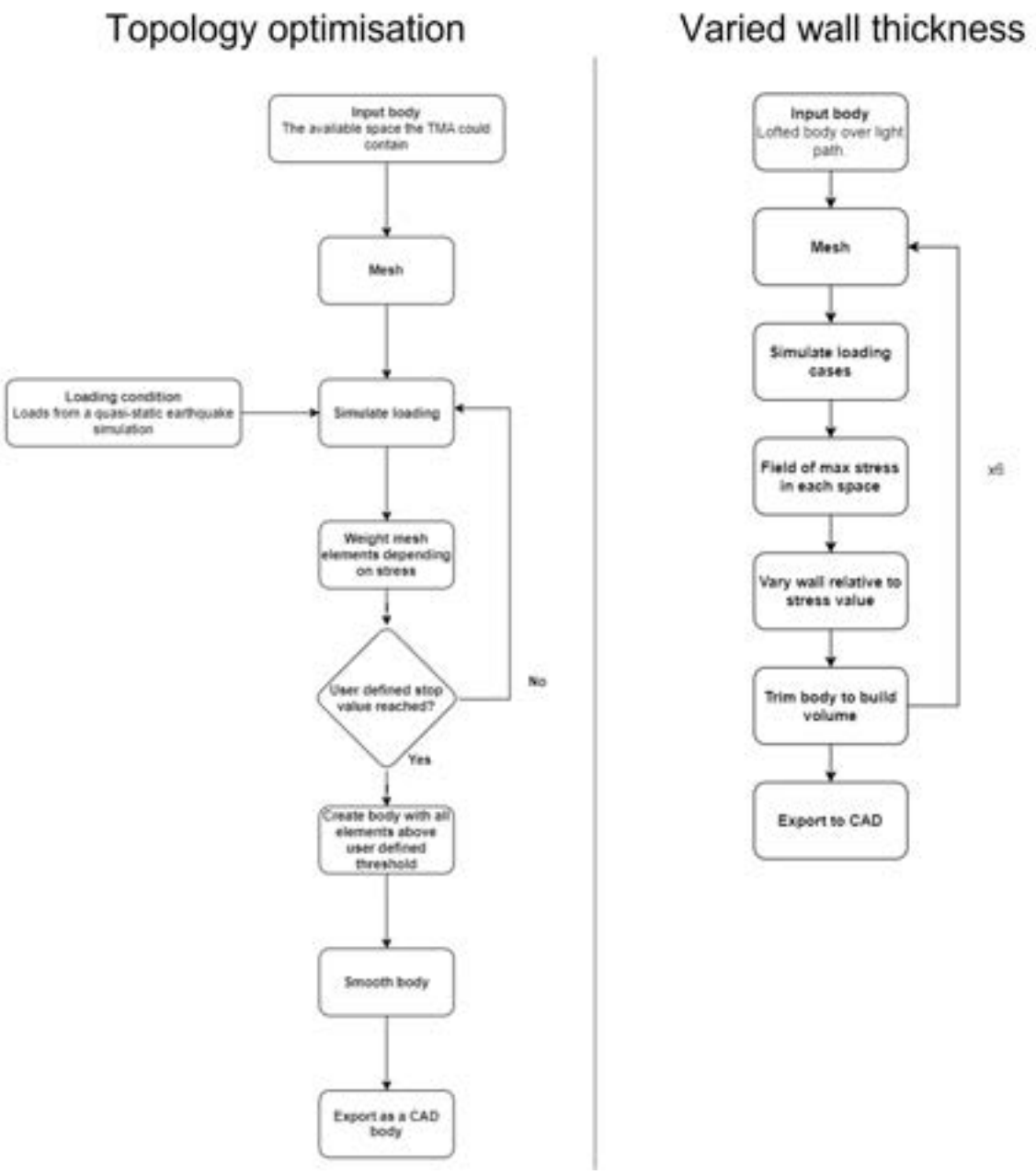

Figure 3. The design for AM process flows: *left* topology optimisation; and *right* the varied wall thickness method.

generated with the elements of the highest weighting, representing a body containing the elements of the most structural significance. The topology optimisation process is presented in Figure 3 *left*.

In this paper, a body representing the available design space for the TMA structure was simulated with the loading condition defined by ESO's quasi-static earthquake analysis on the optical components. It performed this simulation iteratively, altering the weighting of elements each time. Once the simulation reached one of the user-defined stop conditions, shown in Table 2, the simulation ceased. A body was created using the most significant 15% of elements in the build volume. At this threshold, the body was fully connected. This body was then smoothened to remove the roughness from individual elements. This smoothing process altered the geometry of mounting features, so all high-tolerance mounting features were added to the smoothed body in

conventional CAD software.

Figure 4 presents the resulting design for the TMA structure after the topology optimisation process described in Figure 3 and the parameters described in Table 2.

Table 2. Topology optimisation parameters.

Objective constraint	**Response constraints**	**Stop condition**	**Other**
Stress $<$ 136 MPa in each quasi-static acceleration loading case.	Structural compliance under gravity loading.	An objective change of $<$ 0.00005 between iterations.	Boundary cell penalty of 0.75
	Volume fraction.	OR a density change $<$0.001 between iterations	
	Note: weighting of 5:1 volume fraction to compliance.	OR iteration number = 1000	

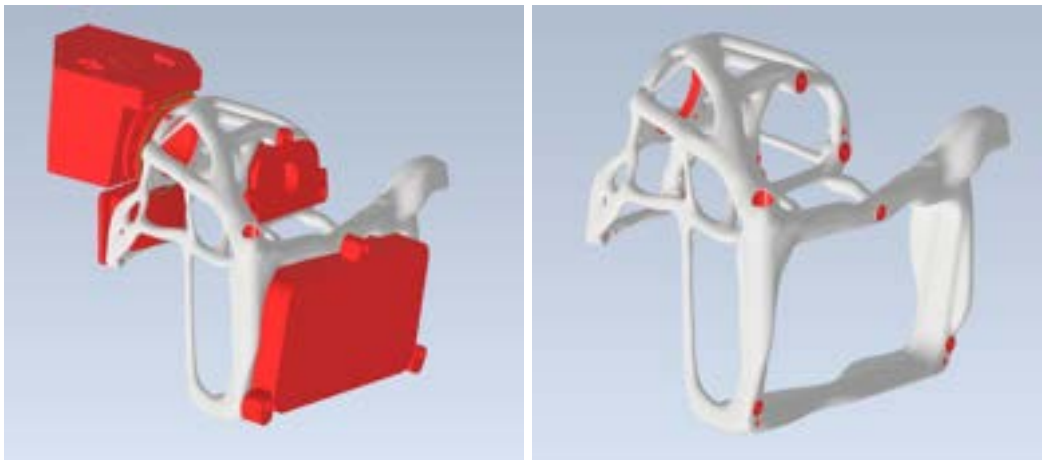

Figure 4. The topology optimised design.

Due to the size of the component, the topology-optimised design would be difficult to manufacture with PBF. With WAAM, small intricate features can fail to print. For this reason, the process would run faster and more reliably with a design with fewer dislocated beams. A design with a more continuous wall would be easier, quicker, and cheaper to manufacture with WAAM.

3.2 Varied wall thickness design

A second design was created, which considered the manufacturing constraints of WAAM. This design was named the varied wall thickness design and used field-driven design. Field-driven designs use fields of data, where each point in a 3-dimensional space is given a value. These data fields are used to drive a design.

The process of creating the varied wall thickness design was similar to the topology optimisation design; however, instead of using the built-in topology optimisation tool, a custom workflow was created. First, a shell surrounding the lightpath of the TMA was created. This had a constant wall thickness of 10 mm. Flanges were added to connect this body to the mounting features of the TMA structure. Then, structural analysis was performed to determine the stress in the body during quasi-static earthquake loading, the same as the loading used in the topology-optimised design. From the multiple load cases of this analysis, a field of maximum stress was created; for all points in the design space, the maximum stress value was recorded from the multiple structural

simulations. The wall thickness of the body was varied relative to the maximum stress field from the structural analysis; where the stress was high, the wall thickness increased; where stress was low, the wall thickness was reduced. The thickness variation was between +5 mm and −2 mm. This process was not constrained to the design space of the TMA structure, which resulted in some local regions exceeding the space available for the TMA structure due to the added wall thickness, so after the wall thickness was varied, the body was trimmed using a Boolean intersection between the new design and a body representing the design space for the TMA. The process of simulation and wall thickness variation was repeated five times to produce a part with a continuous wall of varied thickness. This process could be repeated more times, but after six iterations, the max stress field of the body contained few local peaks, showing the design was distributing the loading efficiently. As with the topology-optimised design, the bodies were exported, and high-tolerance mounting features were added in a conventional CAD software. This design process is presented in Figure 3 *right* and the resulting design can be seen in Figure 5.

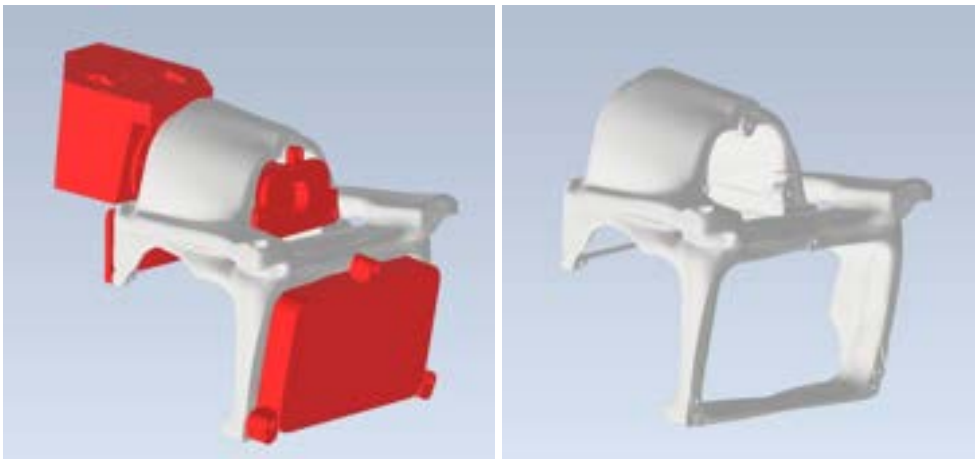

Figure 5. The varied wall thickness design.

A discussion with the National Manufacturing Institute Scotland (NMIS) concluded that the varied wall thickness design provides a good starting point for the investigation of WAAM in ground-based astronomy instrumentation components.

3.3 Design analysis

Both designs were analysed using computer simulation to determine if they could pass the requirements outlined in Table 1. Ansys Mechanical, MATLAB with the Saguaro plug-in and Zemax were used to simulate the performance of the design.

The structural, modal and thermal attributes of designs were assessed using Ansys Mechanical. A fine, tetrahedral mesh of the structure was created. A combination of translational, cylindrical and bonded joint connections were applied between the optical components and the structure to simulate the quasi-kinematic mounting of the optical components. For the standard operation optical study, sliding constraints around the origin of the optical axis were used to allow for the thermal shrinking of the part. A bolt pretension of 6250 N was applied at each mirror flexure, three per mirror. A uniform thermal condition from ambient to 70 K (−203.15 °C) and a gravity acceleration were applied to simulate operational conditions. A fine mesh was applied to all mirror surfaces, and the displacement of nodes was exported. Using the Saguaro MATLAB plugin,[12] the displacements of these nodes were mapped to a grid. This was trimmed to the clear aperture, and the first 25 Zernike coefficients were calculated. The Zernike terms were used to deform the optical surfaces of the TMA Zemax optical model by layering the surfaces. This was used to calculate a wavefront error contribution for the optimised design. Table 3 summarises the results of these simulations alongside the mass of each design in comparison to the machined design.

Table 3. Design analysis results

	Pass criteria	Topology optimised design	Varied wall thickness design
Earthquake loading during operational conditions			
	Maximum stress		
Essential	< 228 MPa	34.8 MPa	150 MPa
Target	< 136 MPa	34.8 MPa	150 MPa
Modal analysis of TMA assembly			
	Minimum Eigenfrequency		
Essential	> 28 Hz	71 Hz	124 Hz
Target	> 70 Hz	71 Hz	124 Hz
Structural, Thermal, and Optical Performance analyses during normal operation			
Wavefront error	< 34 nm	18.6 nm	27.4 nm
Mass comparison			
Conventional machined design		**Topology optimised design**	**Varied wall thickness design**
27.6 kg		16.3 kg	20.1 kg

4. WIRE ARC ADDITIVE MANUFACTURING

The main application for WAAM is for the manufacture of large, small batch components which do not need high tolerance or intricate features,[6] however, high tolerance features can be machined onto a part after print. WAAM is currently under scrutiny by many AM research groups because of challenges with porosity, corrosion, delamination, residual stresses, and oxidation.[13] Aluminium has a high thermal conductivity which removes heat from the weld pool. To sustain a fluid weld pool, higher heat input in the WAAM process is required compared to other metals. This increased heat can cause the evaporation of some alloying metals, such as zinc and magnesium, resulting in porosity.[5]

Porosity is a concern in the application of ground-based astronomical equipment where instruments are housed within vacuum chambers operating at cryogenic temperatures. Porous materials can contain trapped gas and contaminants, which can lead to increased outgassing which can adversely affect neighbouring components. Porosity can also induce cracks, reducing the fatigue life of components.[14] To investigate the porosity and outgassing of WAAM aluminium, eight aluminium alloy 5356 samples were manufactured using a plasma WAAM machine. Two different sample geometries were manufactured, four samples were solid blocks measuring 50 mm $\times$ 50 mm $\times$ 30 mm and another four square walled samples were manufactured measuring 40 mm $\times$ 40 mm $\times$ 25 mm with a wall thickness of 10 mm. Both sample geometries can be seen in Figure 6. One of each sample geometry was separated from its build plate (an aluminium disk it was printed onto) from which X-ray computed tomography data was collected. The other six samples were machined and used for outgas testing. Two of these samples are seen in Figure 7.

4.1 X-ray computed tomography

X-ray computed tomography (XCT) was used on two WAAM samples to assess their porosity. XCT is a non-destructive testing method commonly used in AM to detect and quantify the size and location of internal defects,

Figure 6. The as-printed WAAM sample geometry.

Figure 7. The WAAM aluminium 5356 outgassing samples showing high levels of porosity.

like cracks, pores or voids. The XCT machine used was a Nikon MCT 225. Scan settings of Sample 4 shown in Figure 8 (a) included a helical scan pattern with a voltage of 175 kV, filament current of 175 µA, number of projections of 3141 and a voxel size of 50 µm and a 0.5 mm copper filter. For Sample 8, shown in Figure 8 (b), XCT scan settings included a voltage of 150 kV, filament current of 150 µA, number of projections of 3141 and a voxel size of 35 µm and a 0.5 mm copper filter.

Avizo 2022.1 software was used to convert and down sample the scan data from 32-bit to 8-bit in order to reduce the computing power required for the porosity analysis. The reconstructed XCT scan volume rendering of both WAAM samples can be seen in Figure 8 (b) and (e). Porosity was thresholded using the Otsu method. To focus on pores that have the largest impact on density and to remove noise, pores were filtered to only keep those above 1000 × the volume of the voxel size. The volume fraction, or the percentage of porosity, of Sample 4 was 2.67% before pore filtering and 2.57% after pore filtering. For Sample 8, the volume fraction was 3.83% before pore filtering and 3.70% after pore filtering. X-ray 2D cross sections in Figure 9 show the Z axis dimension of the biggest pore by volume for sample number four (left) and sample number eight (right).

The magnitude of porosity, in terms of size and frequency, is significant within these initial samples. Through discussion with the WAAM provider, it was noted that the gas flow in the vicinity of the arc was higher than required and it is suspected that this high gas flow created turbulence, which resulted in the macro-porosity within the printed samples. However, it should be noted that this was the first attempt by the WAAM provider to print aluminium 5356 and therefore, the project team are confident that with further process development the macro-porosity can be reduced or eliminated.

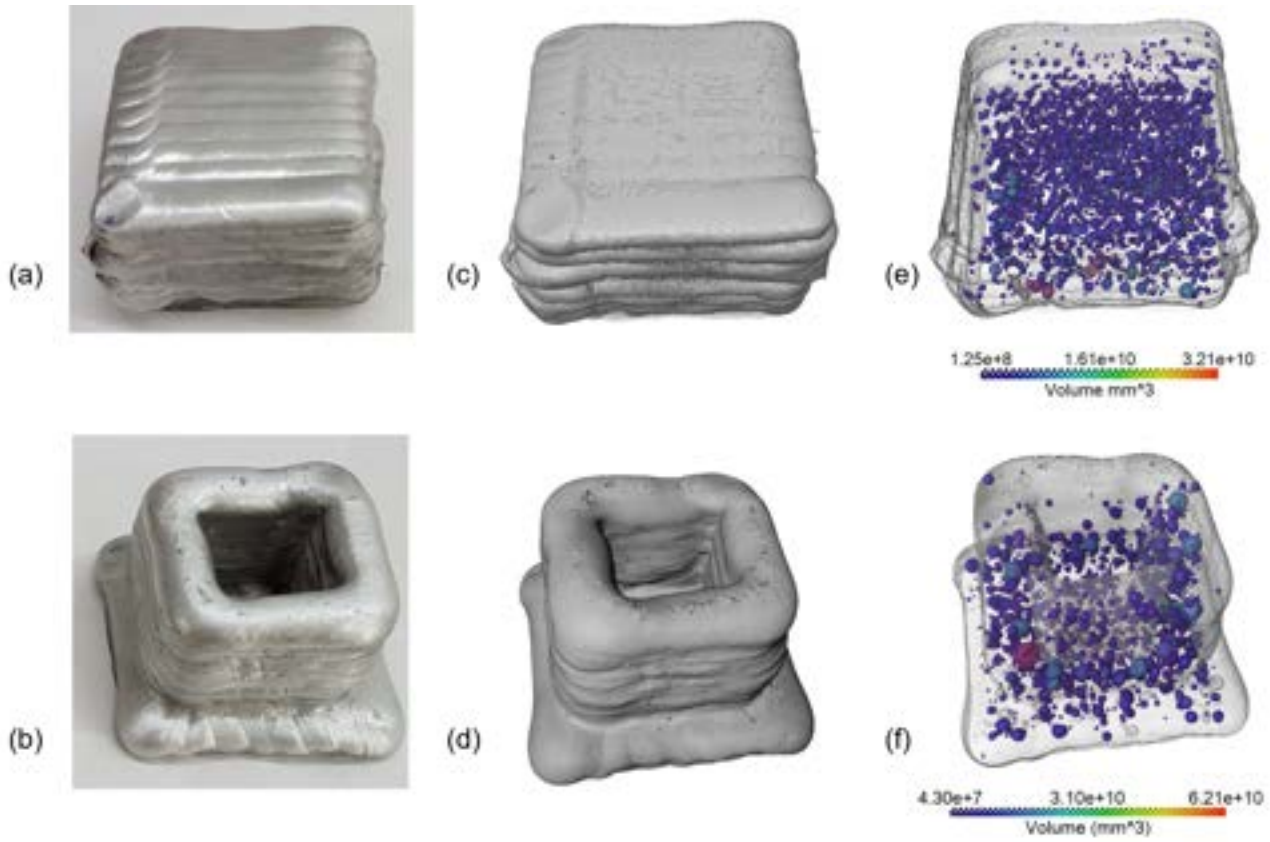

Figure 8. WAAM sample (a) and (b), XCT volume rendering (c) and (d), and porosity analysis (e) and (f).

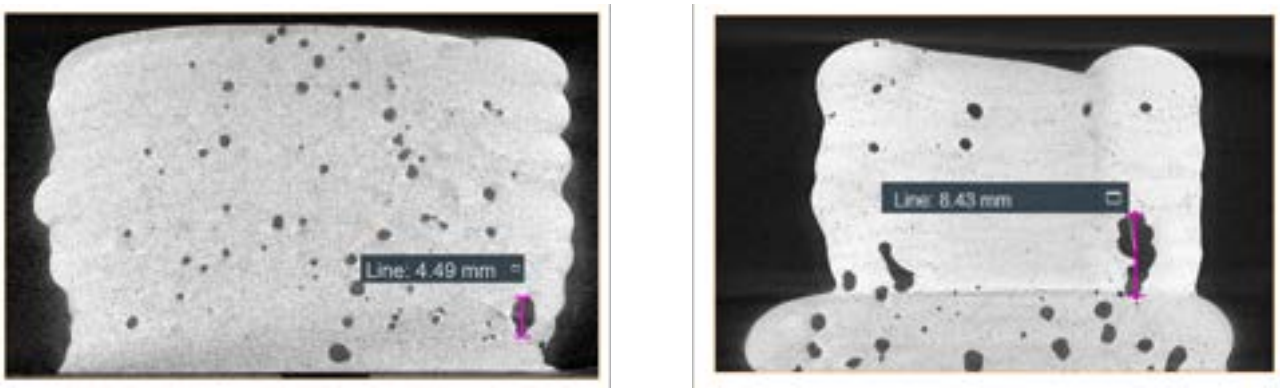

Figure 9. X-ray 2D cross section showing the Z axis dimension of the biggest pore by volume for sample number four (left) and sample number eight (right)

4.2 Outgassing

Outgassing rates were found using the modified throughput method described in *Breen, C., et al. 2022*.[15] In this method, two nominally identical chambers outgas through two orifices into a pumped central volume. Samples were cleaned, dried, then placed under a vacuum ($\approx 10^{-6}$ Pa) within one of the chambers. The second chamber is left empty and is used to accurately subtract the background outgassing rate. The outgassing rates, from pressure data collected during two measurement campaigns, for the six WAAM aluminium 5356 samples are shown in Figure 10. Samples 5, 6, and 7 had 5 mm removed from all faces by CNC machining after printing. Samples 1, 2, and 3 were not machined and have irregular surfaces from the WAAM process. Data from aluminium blanks, parts machined from a block of material and not produced using WAAM, are presented for reference.

A MATLAB script[16] was used to calculate outgassing rates for the samples. Table 4 presents the averaged outgassing rates of the two campaigns at 1 hour and 10 hours. In Figure 10, WAAM Samples 3 (machined) and 7 (non-machined) show a sudden increase in outgassing rate during the measurement. It is thought that the cause of this increase may be due to a trapped volume of gas escaping from an internal pore within the material.

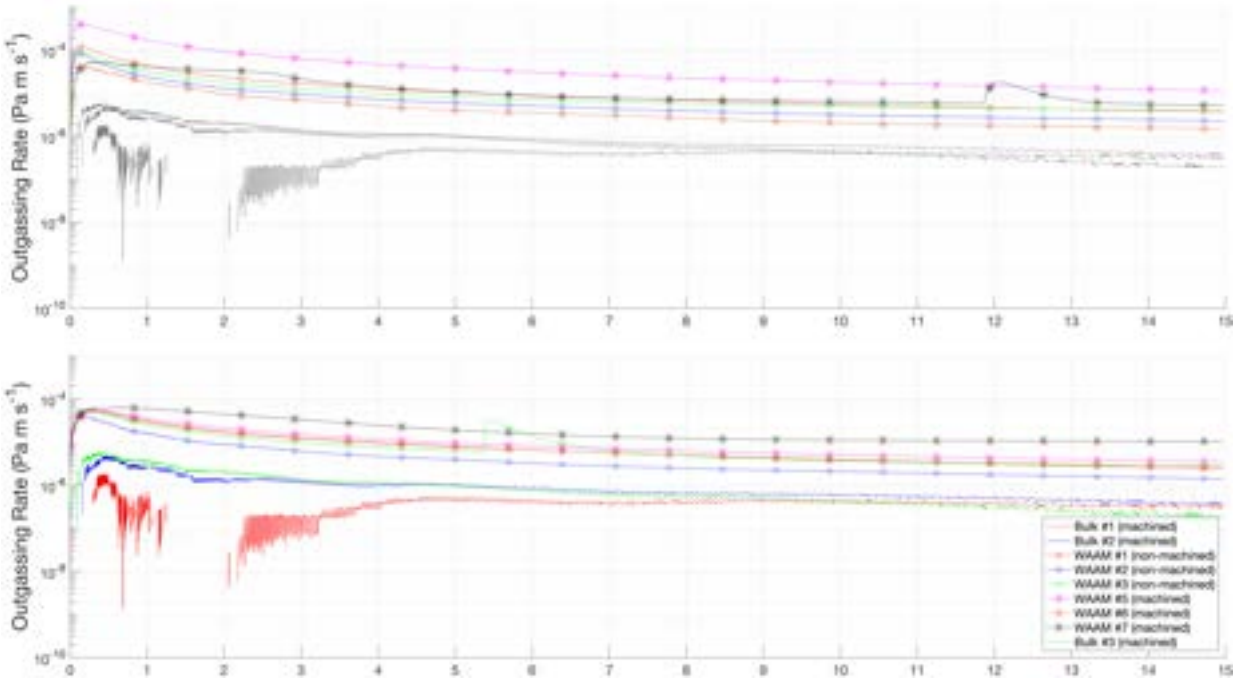

Figure 10. Outgassing rates of six aluminium 5356 wire arc additive manufacture samples: *upper plot*, outgassing data collected in Jun. 2023 (bulk measurements replicated from lower plot); and *lower plot*, outgassing data collected in Aug. 2023.

Figure 10 and Table 4 highlight that the outgassing rates of the WAAM samples are approximately an order of magnitude ($\times 10$) larger than the conventional bulk aluminium samples. Given the externally visible and internally calculated porosity, the increase in outgassing rates is expected. Comparing the machined and non-machined samples, on average the machined samples exhibit a lower outgassing rate than the non-machined. The difference between the machined and non-machined could be a result from the irregular non-machined surface geometry trapping local volumes of air which take longer to outgas; an effect of the increased porosity observed with the XCT in this geometry; and\or an effect from surface deposit, a common artefact of aluminium WAAM and welding.[6] Ultimately, further WAAM samples, with optimised print parameters to minimise porosity, are required to reduce the variables affecting the outgassing rates. If the non-machined samples continued to exhibit high outgassing rates, there would be less benefit gained from WAAM in terms of time and cost if structure required machining of the external skin prior to operation.

5. DISCUSSION

Although designs can be optimised using generative design techniques, the freeform geometries these design algorithms output can be difficult to manufacture using conventional subtractive manufacturing methods. WAAM has yet to be used in ground-based astronomy instrumentation, but could allow the manufacture of complex, freeform geometries in large optomechanical structures. Our initial investigation into WAAM created samples with high levels of porosity, but it provides a path for process development, both in terms of WAAM and AM design. Therefore, with dedicated funding for exploring WAAM in ground-based astronomy, the production of components similar to the TMA is feasible.

Table 4. Outgassing values of six WAAM aluminium 5356 samples averaged over 2 measurement campaigns

Sample ID	Outgassing Rate (Pa m s^{-1})	
	1 Hr	10 Hr
Bulk Aluminium Samples		
1	3.9×10^{-7}	4.1×10^{-7}
2	2.6×10^{-6}	5.6×10^{-7}
3	3.6×10^{-6}	4.1×10^{-7}
Machined WAAM Samples		
1	3.8×10^{-5}	4.7×10^{-6}
2	2.0×10^{-5}	2.6×10^{-6}
3	2.9×10^{-5}	4.3×10^{-6}
Non-Machined WAAM Samples		
5	1.0×10^{-4}	1.1×10^{-5}
6	2.3×10^{-5}	3.0×10^{-6}
7	5.1×10^{-5}	8.8×10^{-6}

Assuming an optimum print process for WAAM aluminium can be achieved, there are further considerations in the production of ground-based astronomy instrumentation components using WAAM. First, a strategy for the machining and post-processing of a WAAM printed component would need to be created. Investigations into tool access for lapping mounting features and material post-processing are needed. In addition, to accurately perform FEA simulations of WAAM aluminium components, an investigation into the material properties of WAAM aluminium in cryogenic environments is required.

6. SUMMARY AND FUTURE WORK

The goal for this project was to investigate a method of introducing function-optimised large ($> 0.5\,\mathrm{m} \times > 0.5\,\mathrm{m} \times > 0.5\,\mathrm{m}$) structural components in ground-based astronomy instrumentation. As a result, two alternative designs for the METIS TMA component have been presented. These designs have been optimised for reduced mass, resulting in designs with one continuous body (30 parts consolidated into 1) instead of the conventional subtractive machined design, which required assembly. One design was optimised using topology optimisation, while another was optimised using a custom generative design process. The latter of these designs is more applicable for manufacturing using WAAM. The first investigation into WAAM aluminium, resulted in samples with high levels of porosity ($\sim 3\% \rightarrow 4\%$) and that outgassed at a higher rate ($\sim 10\times$) than conventional bulk aluminium counterparts.

Future work will investigate methods for reducing the macro-porosity seen within the WAAM samples and creating optimum WAAM print parameters for aluminium. To support this effort, further XCT data at a smaller voxel size has been acquired to aid the quantification of the micro-porosity, which was filtered in this study, as this may identify a new variable to be optimised. Following an optimisation of the WAAM parameters, further samples will be printed to determine the whether the observed high outgassing rates are related primarily to the observed porosity, or the surface deposit and irregular geometry.

7. DATA ACCESS STATEMENT

The CAD files for both the topology-optimised design and varied wall thickness design are openly available from eData, the STFC Research Data repository, at: https://edata.stfc.ac.uk/handle/edata/938.

The raw measurement data (time, pressure & temperature) used to calculate the outgassing rates presented in Section 4.2 are openly available from eData at: https://edata.stfc.ac.uk/handle/edata/943. The MATLAB script used to calculate the outgassing rates from the raw measurement data can be accessed at: https://doi.org/10.5281/zenodo.8348537.

8. ACKNOWLEDGEMENTS

The authors acknowledge the UKRI Future Leaders Fellowship 'Printing the future of space telescopes' under grant # MR/T042230/1 for enabling delivery of this research.

REFERENCES

[1] F42.91-12, "Terminology for additive manufacturing technologies," *ASTM* **10.04** (2012).

[2] Vafadar, A., Guzzomi, F., Rassau, A., and Hayward, K., "Advances in metal additive manufacturing: A review of common processes, industrial applications, and current challenges," *Applied Sciences* **11**(3) (2021).

[3] Frasch, J., Hilpert, E., Hartung, J., Damm, C., and Heidler, N., "Optical housing made by additive manufacturing," in [*Advances in Optical and Mechanical Technologies for Telescopes and Instrumentation V*], Navarro, R. and Geyl, R., eds., **12188**, 121880Y, International Society for Optics and Photonics, SPIE (2022).

[4] Khorasani, A., Gibson, I., Veetil, J. K., and Ghasemi, A. H., "A review of technological improvements in laser-based powder bed fusion of metal printers," *The International Journal of Advanced Manufacturing Technology* **108**(1–2), 191–209 (2020).

[5] Lehmann, T., Rose, D., Ranjbar, E., Ghasri-Khouzani, M., Tavakoli, M., Henein, H., Wolfe, T., and Qureshi, A. J., "Large-scale metal additive manufacturing: a holistic review of the state of the art and challenges," *International Materials Reviews* **67**(4), 410–459 (2022).

[6] Ryan, E. M., Baker, M., Tsakiropoulos, P., Kumar, V., Whiting, M. W., and Watts, J. F., *Large-scale metal additive manufacturing: a holistic review of the state of the art and challenges*, PhD thesis, University of Surrey (2020).

[7] Addilan, "Addilan ARCLAN 1000-5X." https://www.addilan.com/en/addilan-machine/. Accessed: 2023-09-10.

[8] Heidler, N., von Lukowicz, H., Hilpert, E., Risse, S., Alber, L., Klement, J., Heine, F., Bölter, R., and Armengol, J., "Topology optimization and additive manufacturing of an optical housing for space applications," *EPJ Web of Conferences* **215**, 01005 (01 2019).

[9] Frank, C., Hammersley, P., Buzzoni, B., Manescau, A., Arsenault, R., Madec, P.-Y., Birkmann, M., Mueller, M., Salgado, F., Guisard, S., and Kroedel, M., "Design, fabrication, integration and commissioning of an upgraded guiding probe for the VLT unit telescope 4," in [*Advances in Optical and Mechanical Technologies for Telescopes and Instrumentation*], Navarro, R., Cunningham, C. R., and Barto, A. A., eds., **9151**, 915111, International Society for Optics and Photonics, SPIE (2014).

[10] Relativity Space, "Press release: Relativity space maps path to terran r production at scale with unveil of stargate 4th generation metal 3d printers." https://www.relativityspace.com/press-release/2022/10/24/relativity-space-maps-path-to-terran-r-production-at-scale-with-unveil-of-stargate-4th-generation-metal-3d-printers. Accessed: 2023-09-10.

[11] Parr-Burman, P., "Lm spectograph sub-system design and analysis report," tech. rep., The UK Astronomy Technology Centre (2022).

[12] College of Optical Sciences, University of Arizona, "SAGUARO MATLAB plug-in." http://www.loft.optics.arizona.edu/saguaro/downloads/ (Apr 2018). Accessed: 2023-09-10.

[13] Vimal, K., Naveen Srinivas, M., and Rajak, S., "Wire arc additive manufacturing of aluminium alloys: A review," *Materials Today: Proceedings* **41**, 1139–1145 (2021). Advances in Minerals, Metals, Materials, Manufacturing and Modelling.

[14] Tammas-Williams, S., Withers, P. J., Todd, I., and Prangnell, P. B., "The influence of porosity on fatigue crack initiation in additively manufactured titanium components," *Scientific Reports* **7**(1) (2017).

[15] Breen, C., Walpole, J., Atkins, C., McPhee, S., Cliffe, M., Moffat, J., Edwards-Mowforth, M., Lister, I., Reynolds, L., Conley, A., Allum, S., Snell, R. M., Tammas-Williams, S., and Watson, S., "Outgassing properties of additively manufactured aluminium," in [*Advances in Optical and Mechanical Technologies for Telescopes and Instrumentation V*], Navarro, R. and Geyl, R., eds., **12188**, 121882I, International Society for Optics and Photonics, SPIE (2022).

[16] Breen, C., "breenci/am4space_outgassing: Code for 'Lightweighting large optomechanical structures in astronomy instrumentation utilising generative design and additive manufacturing'." https://doi.org/10.5281/zenodo.8348537 (Sept. 2023).